REPORT DOCUMENTATION PAGE

Form Approved
OMB No. 0704-0188

1. REPORT DATE (DD-MM-YYYY)	2. REPORT TYPE	3. DATES COVERED (From - To)
18-07-2003	Technical Abstract	

4. TITLE AND SUBTITLE

Multi-Scale Approach to Investigate the Tensile and Fracture Behavior of Nano Composite Materials

5a. CONTRACT NUMBER

5b. GRANT NUMBER

5c. PROGRAM ELEMENT NUMBER

6. AUTHOR(S)

C.T. Liu

5d. PROJECT NUMBER
2302

5e. TASK NUMBER
0378

5f. WORK UNIT NUMBER

7. PERFORMING ORGANIZATION NAME(S) AND ADDRESS(ES)

Air Force Research Laboratory (AFMC)
AFRL/PRSM
10 East Saturn Blvd.
Edwards AFB CA 93524-7068

8. PERFORMING ORGANIZATION REPORT NUMBER

AFRL-PR-ED-AB-2003-196

9. SPONSORING / MONITORING AGENCY NAME(S) AND ADDRESS(ES)

Air Force Research Laboratory (AFMC)
AFRL/PRS
5 Pollux Drive
Edwards AFB CA 93524-7048

10. SPONSOR/MONITOR'S ACRONYM(S)

11. SPONSOR/MONITOR'S NUMBER(S)
AFRL-PR-ED-AB-2003-196

12. DISTRIBUTION / AVAILABILITY STATEMENT

Approved for public release; distribution unlimited.

13. SUPPLEMENTARY NOTES

For presentation at the AFOSR Materials and Mechanics Program Review in Santa Fe NM, taking place 8-10 September 2003.

14. ABSTRACT

15. SUBJECT TERMS

16. SECURITY CLASSIFICATION OF:			17. LIMITATION OF ABSTRACT	18. NUMBER OF PAGES	19a. NAME OF RESPONSIBLE PERSON
a. REPORT	b. ABSTRACT	c. THIS PAGE			Leilani Richardson
Unclassified	Unclassified	Unclassified	A	7	19b. TELEPHONE NUMBER (include area code) (661) 275-5015

MULTI-SCALE APPROACH TO INVESTIGATE THE TENSILE AND FRACTURE BEHAVIOR OF NANO COMPOSITE MATERIALS

Dr. C. T. Liu
AFRL/PRSM, 10 E. Saturn Blvd.
Edwards AFB CA 93524-7680
Tel. No. 661-275-5642; Fax No.661-275-5435
E-Mail Address: chi.liu@edwards.af.mil

Narrative Description of the Program:

This program is concerned with the effects of nano size particles on the tensile and fracture behavior of particulate composite materials. The program's basic approach involves a blend of experimental and analytical studies. In general, mechanisms and mechanics involved in the damage process and cohesive fracture are emphasized. Special issues that will be addressed are: (1) To what extent and by what mechanism the nano size particles affect damage initiation and evolution processes, deformation process, and crack growth behavior? (2) What are the deformation and failure mechanisms on the meso and the macro levels? (3) How the nano size particles affect the characteristics of the interphase between the particle and binder? And what is role of the interphase properties in damage initiation and evolution processes?

The objectives of the proposed research are to (1) obtain a fundamental understanding of the effects of nano size aluminum particles on the constitutive and crack growth behavior of particulate composite materials, (2) investigate the effects of aluminum particle size on deformation mechanism, damage process, hysteresis, and fracture strength under a constant strain rate condition, (3) determine the role of interphase in damage initiation and evolution processes, (4) determine the deformation and failure mechanisms on meso and macro scales, (5) develop a microstructure and statistics based technology to evaluate the inherent material quality ,and (6) provide guidance for developing high strength nano solid propellants.

In this program, Uniaxial tensile tests will be conducted on specimens with and without pre-crack to determine the constitutive and fracture behavior under a constant strain rate condition. Digital Image Correlation techniques will be used to determine the strain field on the surface of the specimen. Ultrasonic and high-resolution x-ray radiograph techniques will be used to determine the damage initiation and evolution processes in the material. The correlation of the damage state and the constitutive and fracture behavior will be determined. Statistical mechanics and fracture mechanics will be used to determine the inherent quality of the material. Multi-scale numerical modeling techniques will be used to simulate the damage and fracture processes in the material. In addition, damage mechanics, on the meso- scale, and fracture mechanics, on the macro-scale, will be used to simulate the crack growth behavior.

Detailed Technical Approach for FY03:

In FY 03, there are three major tasks: Task 1 – Meso and Macro Scales Strain Measurements, Task 2 – Multi-Scale Modeling on damage Initiation and evolution, and Task 3 – Cumulative Damage Analysis

Task 1 – Meso and Macro Scales Strain Measurements:

In the first phase of this program, the deformation and failure mechanisms in two matrix materials (Solithane 113, TPEG) and a composite material (TPEG with 10% by weight of aluminum particles) were investigated. Uniaxial tensile specimens were made from the three materials. Tests were performed in a Hitachi scanning electron microscope (model S-2460N), which equipped with a displacement controlled loading device which crosshead can travel continuously. The application of Speckle Interferometry with Electron Microscopy (SIEM) consists of three procedures: the creation of micro/nano speckles on the specimen surface, recording and digitization of the speckle patterns before and after specimen deformation, and deformation analysis of the speckle patterns using an efficient program called CASI (Computer Aided Speckle Interferometry).

The selection of speckle size is determined by the size and deformation magnitude of the specimen and the image magnification selected. For this particular study, four different magnifications were used: 40x, 80x, 200x, and 1500x. SiC particles of about 1 μm in size were used for all the first three magnifications and physical vapor deposition process was used for the last magnification. The speckle size for the 1500x was about 0.2 μm. The digitally recorded speckle patterns before and after deformation were subdivided into 32×32 pixels array subimages. A corresponding pair of subimages was "compared" through the CASI software (a 2-D two-step FFT) to yield the displacement vector averaged over the subimage. The physical size of a pixel is a function of the magnification and the total number of pixels with the recorded image. In the current system the image size is 4.5 in. × 3.5 in. digitized with a 2048 × 2048 pixels array. For a 1500x image, the resulting physical size of a pixel is 37 nm in x (or horizontal) and 29 nm in y (or vertical) directions. CASI usually has a 0.5 pixel displacement resolution. Thus, the sensitivity of SIEM at this magnification is about 19 nm in x and 15 nm in y directions, respectively. CASI calculation gives displacement components directly. Strains are obtained via appropriate displacement-strain relations.

Experimental findings revealed that the strain distributions varied with the size of the area, A, in which the data were analyzed. The area, A_u, in which the strain distributions was relatively uniform, or the material's microstructure had no significantly effect on the strain distributions, varied with the three materials investigated. The sizes of A_u for Solithane 113, TEPG, and the composite material were 1.04 mm^2, 0.01 mm^2, 0.074 mm^2, respectively. These experimental observations reveal that there exists a length scale below which the material's microstructure has a significant effect on the strain distributions. In other words, a representative area, which is defined as an area in which the material's microstructure has no significant effect on the strain distribution, exists for the materials investigated in this study. It is interesting to point out that for the three materials investigated, the normal strain distributions measured in a small area of 0.002 mm^2 at 1500X are highly nonuniform and both tensile and compressive strain fields exist (Figs.

1, 2, and 3). In addition, for Solithane 113 and the composite material, positive transverse strains were developed at certain locations in the materials. The triaxial tensile strain fields are the potential failure locations in the materials.

In addition to determining the strain fields, the damage mechanisms near the crack tip were also investigated. Although the deformation mechanisms, large displacement and ligament formation, near the crack tip of the three materials were similar, the damage mechanisms near the crack tip depended on the material. For Solithane 113, a highly damaged region was developed at the crack tip (Fig. 4). Inside the damage region, through-thickness voids were formed. The crack growth mechanism involved voids formation ahead of the crack tip and the coalescence of the main crack tip with the void. For TPEG, no through-thickness voids were formed near the crack tip. Instead, microcracks were formed in the ligaments (Fig. 5). The growth of the microcrack resulted in the fracture of the ligament. For the composite material, voids were formed around the AL particles (Fig. 6). As the applied strain was increased, the void elongated, resulting in a higher toughness of the material and slow crack growth rate.

Task 2 – Multi-Scale Modeling on Damage Initiation and Evolution

Progressive damage in the specimen was simulated using a multi-scale technique. In this approach, the macro-level (i.e. composite specimen level) and the micro-level (i.e. the particle and matrix material level) are interconnected in analysis in a staggered way. First of all, the effective composite material properties are computed from the particle and matrix material properties, and the macro-analysis (i.e. composite structural analysis) is performed to calculate composite stresses and strains using the finite element method. The stresses and strains at the composite structural level are decomposed into the stresses and strains at the base material level, i.e. particles and matrices. Then, damage initiation and propagation are described for the particle and matrix materials. In the present study, only matrix damage is considered because the particles a very strong compared to the matrix. Therefore, matrix cracking is the main damage parameter. The damage discussed from now on is matrix damage. When the degraded matrix material properties are computed from a damage theory, effective composite material properties are computed from the particle and degraded matrix material properties. This iteration process of computation continues as long as the damage continues to grow or until the applied load reaches the designated level.

The results of numerical modeling analysis revealed that as sporadic damage grew, damage saturations were reached at certain applied strain levels. The saturation of damage implied that a crack was formed. However, the developed cracks did not propagate beyond a certain length. In other words, there were non-propagating cracks developed in the specimen. When the applied strain was increased, the non-propagating cracks coalesced to form a longer crack, which propagated and caused specimen fracture. This computer simulated damage initiation and evolution processes as well as crack growth behavior agreed well with experimental observation.

Figures 7, 8, and 9 show macro-normal stress, macro-normal strain, and damage distributions in grayscale at the strain level close to specimen failure. Because matrix failure is the main damage in the composite, the matrix stress and the damage plots show some correlations, especially at the highly accumulated damage locations. The major damage locations are also well illustrated in

the Macro-strain plot. However, the macro-stress plot does not indicate any clear damage location. By comparing Fig. 8 with Fig. 9, on the first approximation, the large strain zones are equivalent to the size the non-propagating cracks.

Task 3 – Cumulative Damage Analyses:

Throughout the loading history, the progressive development and interaction of various damage modes change the state of the material, or the mechanical response of the material. In general, when the particulate composite material is tested under a constant strain rate condition, the initial linear portion of the stress-strain curve is associated with a stretching on undamaged material, with the filler particles bonded to the binder. As the external load is continuously increased, at a certain critical stress level, dewetting occurs. When the density of the dewetted particles reaches a critical value, the rigidity of the material is thereby reduced, and usually this critical dewetting state coincides with the transition from linear response to nonlinear behavior. As the specimen is continuously stretched, the number of dewetted particles is increased, and the formed voids start to grow and coalesce. This damage process is related, primarily, to the nonlinear response of the material, and it can be characterized by bulk volume change during stretching. The bulk volume change during straining is usually known as the strain dilatation, which is partially caused by the nucleation of new voids, and partially caused by the growth of the existing voids. The extent of the volume dilatation depends on the nature of the binder/particle system, the testing temperature, and the strain rate. Therefore, to effectively use the material in structural applications one needs to understand the damage initiation and evolution processes, the effects of damage and crack development on the material's response, and the remaining strength and life of the structures.

In this task, a linear cumulative damage theory was used to derive a time-dependent damage parameter, $D(t)=\left[\int_0^t \sigma^{\beta}\, dt\right]^{1/\beta}$. Currently, we are developing a time-dependent cumulative damage model and determining the correlation of the cumulative damage and the constitutive behavior of a solid propellant.

In addition to developing a phenomenological cumulative damage model, Lockheed-Martin Research laboratory's High Resolution Digital X-Ray Systems were used to monitor the microstructure change, damage process, and volume dilatation under an incremental strain condition. At the time of this writing, we are analyzing the test data to determine the aforementioned parameters as functions of the applied strain.

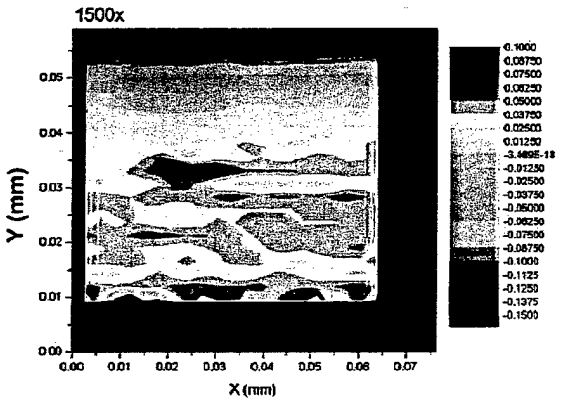

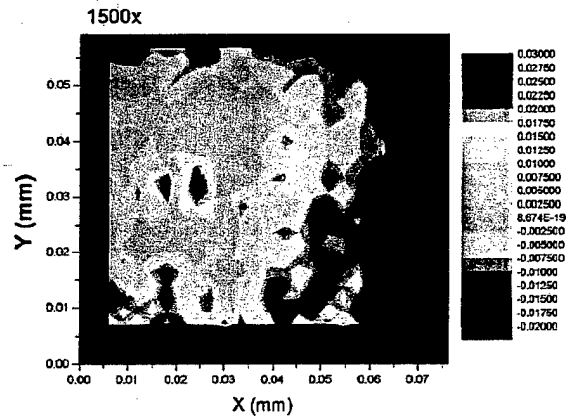

(a) **εyy** (b) **εXX**

Figure 1 Strain Distribution (Solithane 113)

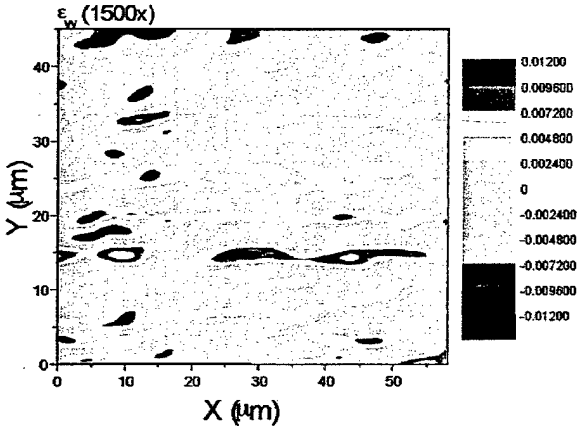

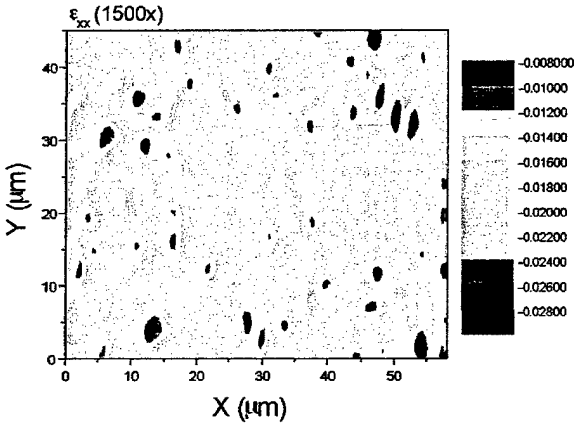

(a) **εyy** (b) **εXX**

Figure 2 Strain Distribution (TPEG)

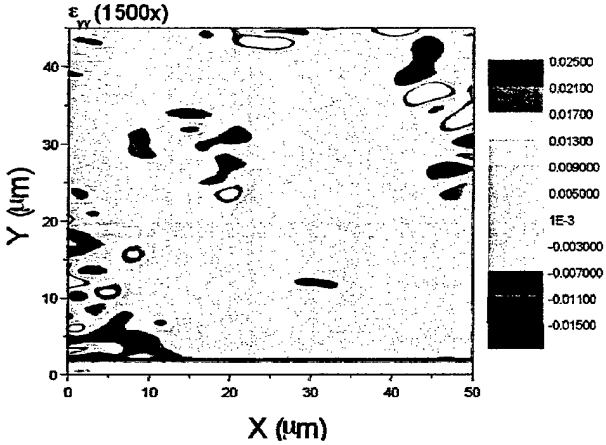

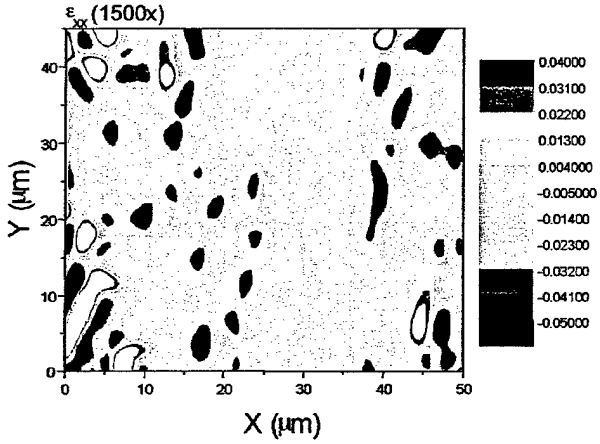

(a) **εyy** (b) **εXX**

Figure 3 Strain Distribution (Composite Material)

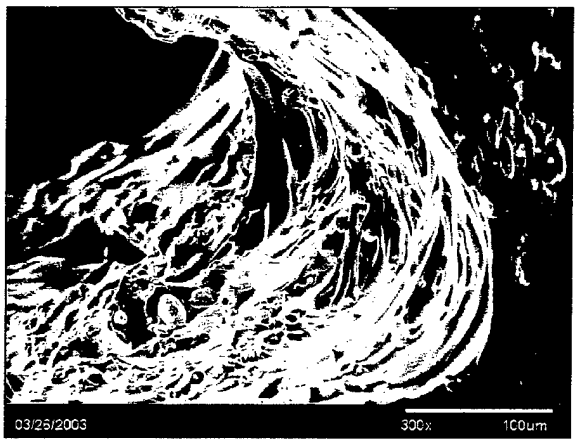

Figure 4 Local Deformation and Failure Mechanisms (Solithatne 113)

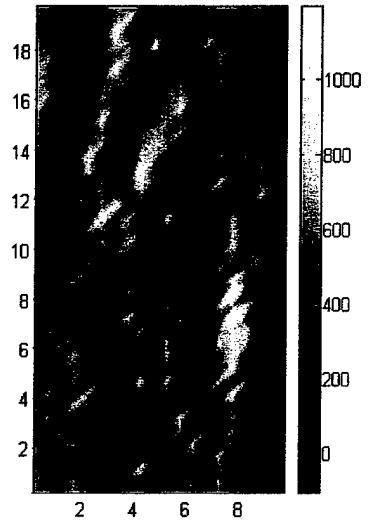

Figure 5 Local Deformation and Failure Mechanisms (TPEG)

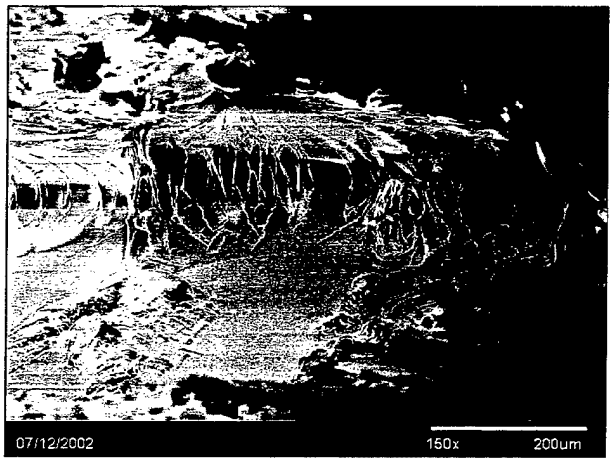

Figure 6 Local Deformation and Failure Mechanisms (Composite Material)

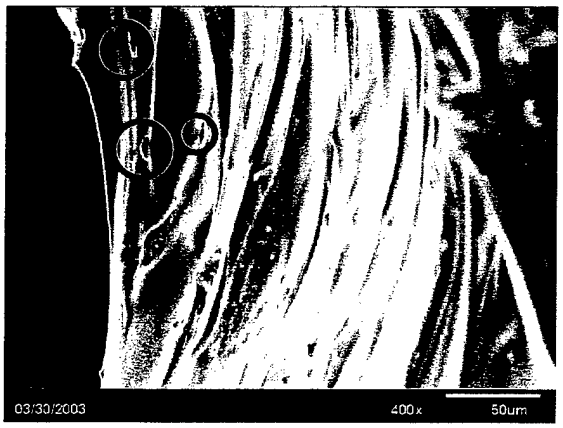

Figure 7 Macro- Normal Stress Distribution

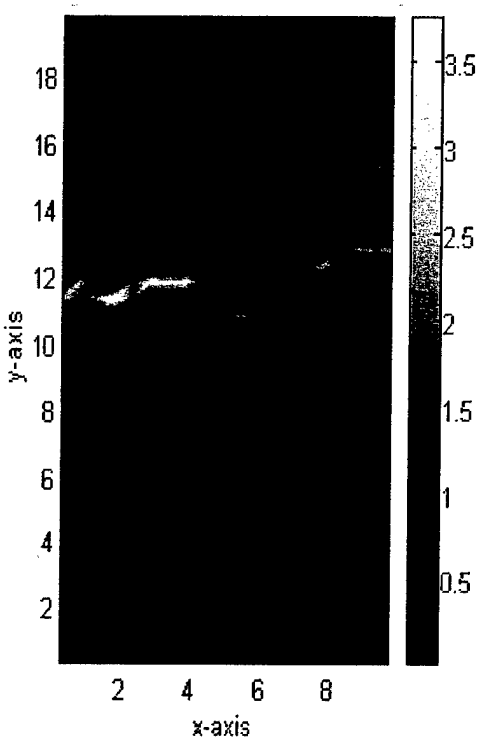

Figure 8 Macro- Normal Strain Distribution

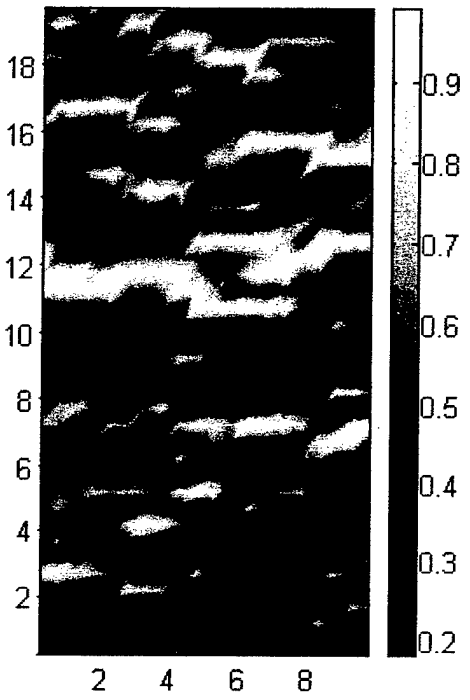

Figure 9 Damage Distribution